Fundamentals of EMPT-Welding[*]

A. Elsen[1], M. Ludwig[1], R. Schaefer[2] and P. Groche[1]

[1] Institute for Production Engineering and Forming Machines, Darmstadt University of Technology, Darmstadt, Germany
[2] PSTproducts GmbH, Alzenau, Germany

Abstract

A well-suited solid state welding process for treatment of tubular structures is the electromagnetic pulse welding technique (EMPT): A pulsed magnetic pressure loads the structure to be welded within a few microseconds and accelerates one of the both contact partners (the so called "flyer") onto a stationary one. When the flyer strikes the stationary contact partner, contact normal stresses far above 1000 MPa act on the interfacial zone between flyer and stationary part. As a result of these high interfacial loads, a layer of several micrometers thickness next to the interface is severely plastically strained. Hence, the oxide layers covering both contact partners are cracked. These chipped oxide particles are blown out of the joining area by a so called "jet". This jet is caused by the air between the two joining partners being compressed and accelerated due to the movement of the flyer. The result of both phenomena –the oxide chipping by severe plastic deformation of the interfacial zone and the particle blow out caused by the jet– is a pure metallic interfacial zone, loaded by contact normal stresses. The conjunction of the highly reactive metallic surface and the contact normal stresses establishes a metallic bonding, whose strength equals at least the strength of the weaker contact partner.

This report presents the results of a collaborative research project between the Institute for Production Engineering and Forming Machines (PtU) and PSTproducts GmbH. Experimental welding analysis is accompanied by numerical work for the study of the underlying mechanisms of solid state welding with respect to interfacial plastic deformation and contact loads. Additional metallographic work gives insight into the microscopical structure of the interfacial joint zone.

Keywords

Welding, Interface, Waviness, Finite element method (FEM)

---

1 Introduction

The electromagnetic pulse welding (EMPW) process allows for the integral joining of conductive metallic components without the addition of thermal energy [1]. For this the components to be joined are accelerated towards each other by a pulsed high-energetic magnetic field to form a solid state cold weld. Unlike thermal welding processes no influence on the microstructure due to heat effects occurs. Moreover the EMPW process offers the potential to join dissimilar and conventionally non-weldable material combinations, such as aluminum and steel, thus enabling the application of light and robust material combinations.

The electromagnetic pulse technology (EMPT) physically bases upon the utilization of electromagnetic body forces (Lorentz force) [2]: Alternating currents in a coil induce a current in a second coil in vicinity of the live coil. The induced current creates a corresponding magnetic field that strongly repels that of the live coil. Hence a tubular conductive part functions itself as a single-winded coil. High currents (> 100 kA) generate a strong force between the tube and the outer coil, which can overcome the yield strength of the work piece. With the help of magnetic field concentrators ("field shapers") the repelling force can be directed to create permanent deformation of the component to a desired shape.

Regarding welding processes, a flyer tube is accelerated by electromagnetic pressure to impact with a tapered base insert at an adequate impact angle (Figure 1). The high impact pressure sweeps off the surface oxide film and forms an atomic bond between flyer and base tubes [3].
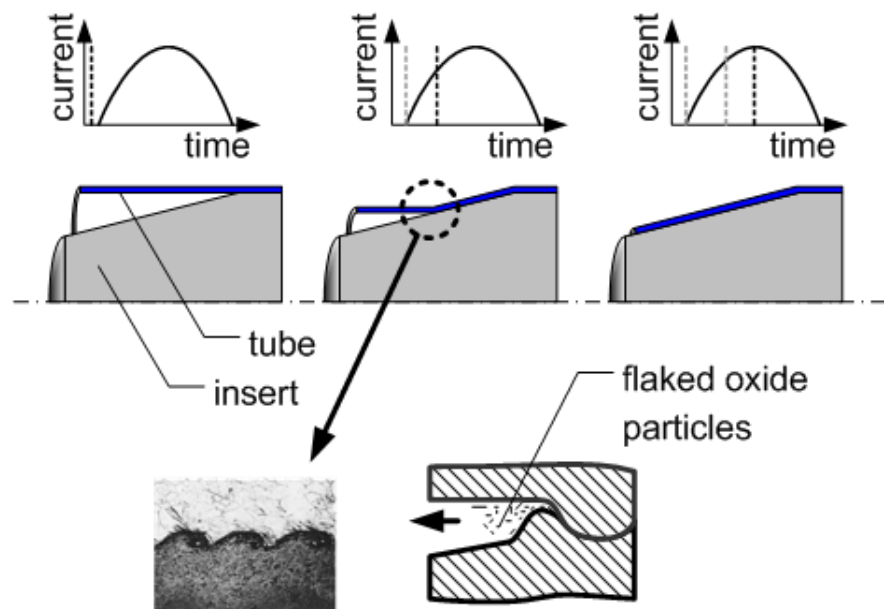

Figure 1: Schematic illustration of electromagnetic pulse welding

2 Experiments

Several experiments have been carried out to identify the influencing parameters on the evolution of the adhesively joined bonds and the characteristic waviness of the interface. A capacitor bank is discharged at a current of 930 kA and a frequency of 14 kHz through a

coil. Based on the geometry of coil and workpieces, this results in a magnetic pressure of 400 MPa onto the surface of the flyer. The material for the cast and machined insert and the outer extruded tube is EN AW-6061-T6 (AlMg1SiCu) (see Table 1 for mechanical properties and Table 2 for the chemical composition).

Alloy	$R_{p0.2}$ [N/mm²]	R_m [N/mm²]	A [%]
EN AW-6061 T6	240	260	9

Table 1: Mechanical properties of Al 6061 T6

Alloy	Si	Fe	Cu	Mn	Mg	Cr	Zn	Ti
EN AW-6061 T6	0.40-0.8	0.7	0.15-0.40	0.15	0.8-1.2	0.04-0.35	0.25	0.15

Table 2: Chemical composition of Al 6061 T6

The experimental setup consisting of a coil, a split field shaper and a specimen holder, which allows for aligning tube and insert inside the coil, can be seen in Figure 2. The capacitor bank is not displayed.
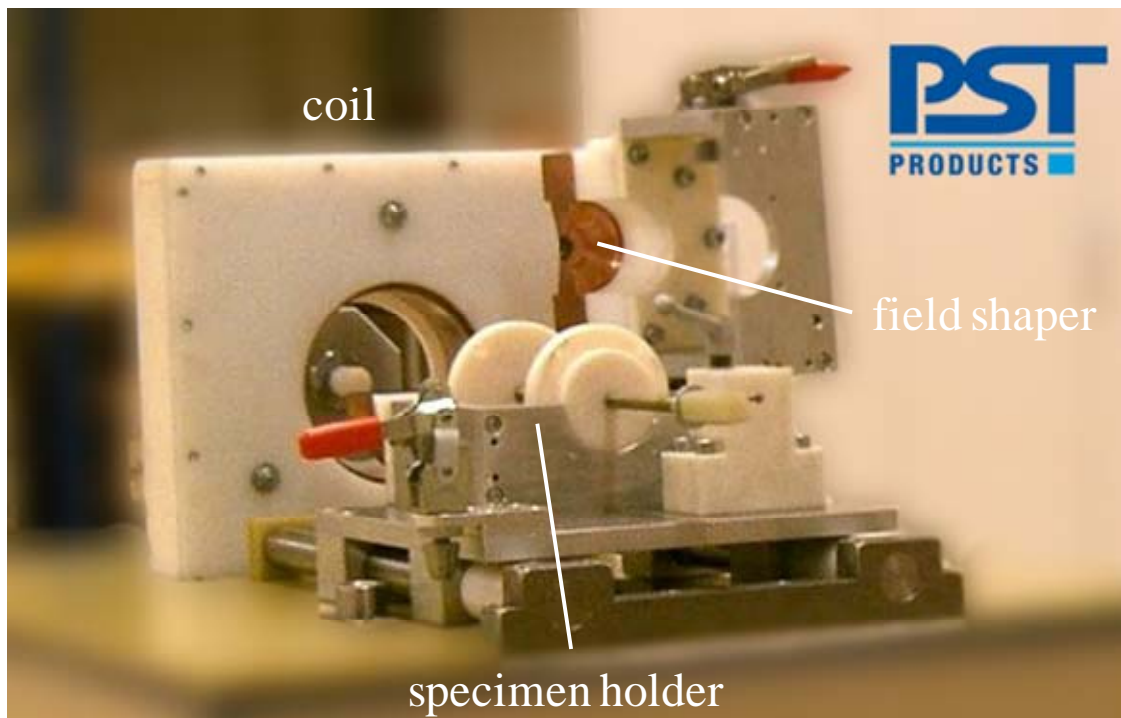

Figure 2: Experimental setup

The geometries and schematic alignment of tube and insert are shown in Figure 3. The aluminum tubes have an outer diameter of 50 mm and wall thicknesses of 1.5 mm, 2.0 mm or 3.0 mm, respectively. The section of the insert that is placed inside the tube has a length of 25 mm and a diameter of 50 mm less twice the wall thickness of the corresponding tube. After 5 mm there is a bevel of either 1 mm or 3 mm ("offset") at an angle of 30°. Inlet and outlet are rounded down to R1 and R0.5. The actual effective area

for the welding process is the tapered part of the insert, angled at either 5°, 7.5° or 10° in the different experimental series.
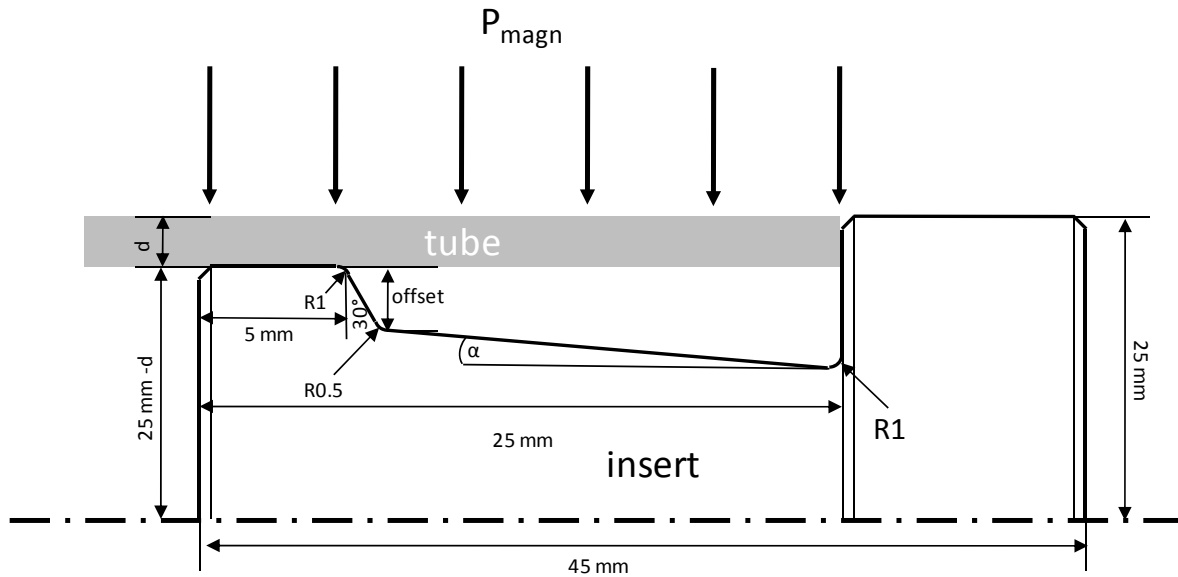

Figure 3: Schematic setup of the welding experiments

Each specimen has been cut through the longitudinal axis to examine the resulting welding length. The plots of the welding lengths in dependency of the wall thicknesses of the outer tubes in Figure 5 show a direct relationship between these parameters and the resulting welding length.
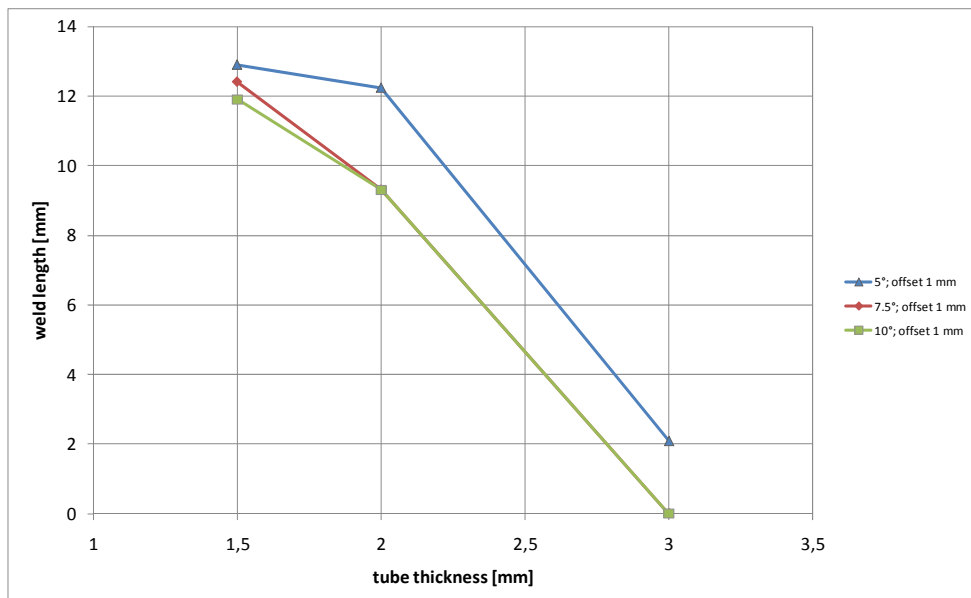

Figure 4: Welding length in dependency of the tube thickness for an offset of 1 mm

In general, the length of the welded joint decreases with increasing wall thickness of the tube. As the deployed magnetic energy is constant for all experiments, an increasing wall thickness results in a lower contact pressure between tube and insert as more energy is

consumed for the compression of the outer tube and the mass inertia of a heavier flyer tube is higher. Due to the velocity of the line contact being subject to the trigonometrical relation $v_{welding} = v_{impact} / \tan(\alpha)$, the lower impact velocity of the flyer results in a lower velocity of the line contact. The angle of the tapered section, which determines the contact angle of flyer and insert, has in this test series only minor influence on the resulting welding length, as the angles of 5°, 7.5° and 10° are already empirical values for sound welding results obtained from previous experiments. Noticeable is the fact that the experiments with an offset of 3 mm and a contact angle of 5° (Figure 5) did not result in a bond no matter the wall thickness. However, the specimen with 7.5° and 10° did weld with tubes of a wall thickness of 1.5 mm and 2.0 mm, while a wall thickness of 3 mm and an offset of 3 mm did not induce a bonding in any variation of the angle. Further investigations of the samples lead to the insight that the flyer tube had bounced off the insert at the low contact angle of 5°. Though the contact pressure was sufficient the contact angle did not result in a continuous line contact and thus in a weld joint.
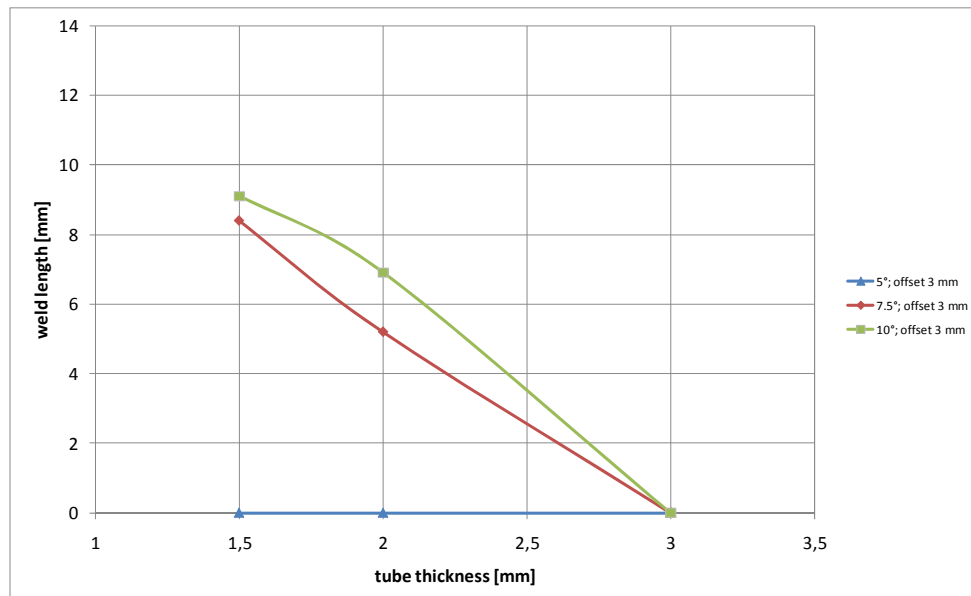

Figure 5: Welding length in dependency of the tube thickness for an offset of 3 mm

3   Metallographic Examination of the Welded Interface

For the investigation of the welded interface, metallographic microsections have been made by embedding the specimen in epoxy resin and subsequently grinding and polishing down to a graining of 0.25 µm. Etching with 1% hydrofluoric acid uncovers the grain boundaries and the welding interface. Figure 6 shows a weld interface with characteristic waviness.
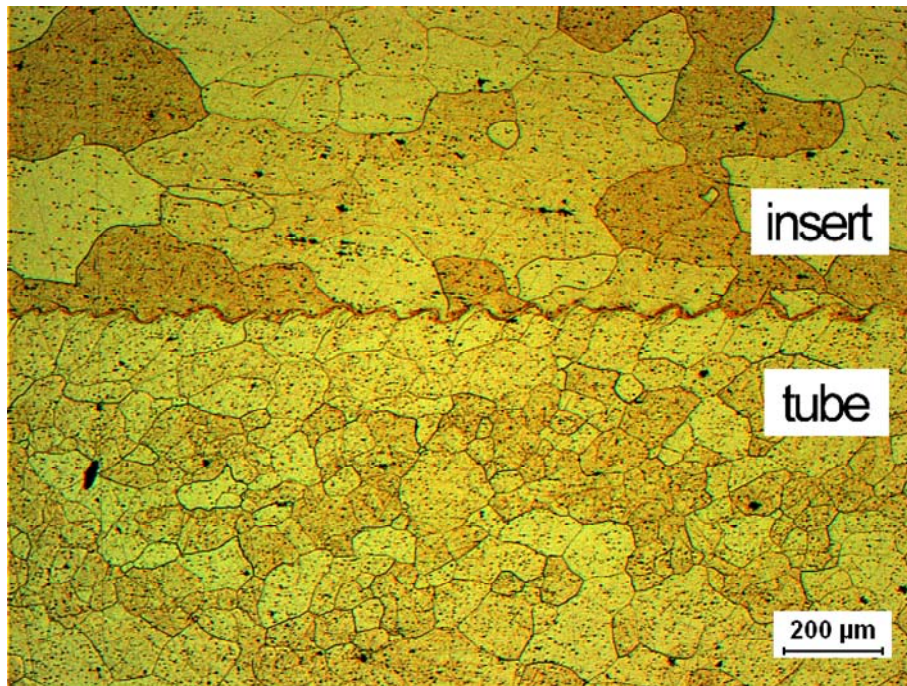
Figure 6: Weld interface with characteristic waviness

The insert exhibits a typical cast structure with large grains compared to the microstructure of the drawn tubes. Within the welding zone the grains are to some extend severely deformed in direction of the advancing line contact (see Figure 7). These specimens have been treated with Weck's etching solution to obtain a color contrast between grain boundaries and the welding interface.
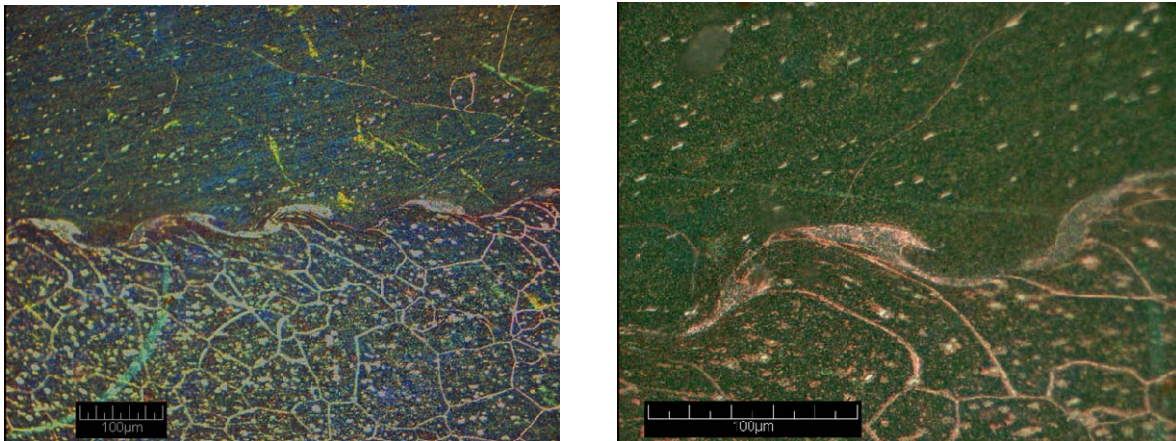

Figure 7: Welding Zone of Al6061-Al6061

Among others a theory based on the Kelvin-Helmholtz instability mechanism in fluid dynamics describes the wave formation as a result of flow velocity discontinuities across the interface [4]. Immediately after impact instabilities close to the severely deformed interface occur, caused by the different velocities of the interacting parts. Material close to the interface has to move faster across the wave hump than material more distant. According to Bernoulli's principle the pressure above a wave is lower than in the vicinity as a consequence of the higher velocity of the surrounding fluid. Hence there is a force that

pulls the crest upwards. The fluids nearby the wave trough behave analogously. Material yields more slowly across the surface of a wave trough than in its proximity, therefore the pressure is locally increased causing the wave trough to be pressed downwards. Refer to [5] for further details on this theory on the wave formation.

In Figure 8 a numerical simulation of a spatial Kelvin-Helmholtz-instability is compared to a microsection of a weld interface. Periodic sequences of sinusoidal waves and turbulent vortices can be observed in both the numerical simulation and the microsection of the specimen. This indicates that the theory of wave formation being an effect similar to the turbulent flow in fluids moving at different speeds is plausible.
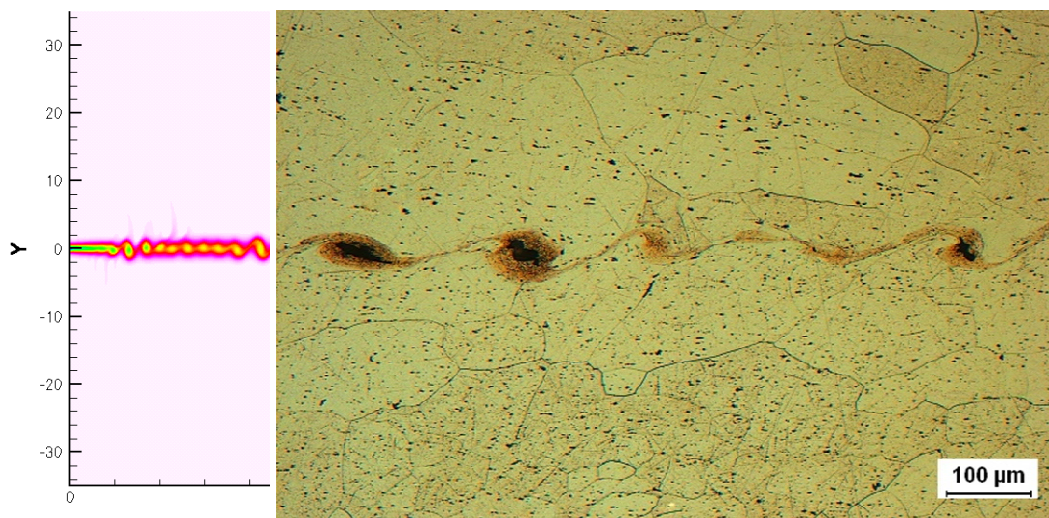

Figure 8: Numerical simulation of a spatial Kelvin-Helmholtz-instability (left) compared to a microsection of a weld interface of Al-Al (right)

4   Numerical Simulations of the Impact Zone

The finite element discretization of the EMPT-process is very challenging. Especially in the welding zone where very high strain rates occur the elements in the contact are underlying great distortions. However, with the help of adaptive meshing in this zone the process can be simulated. Figure 9 shows the setup of the simulation model.

The simulation is an explicit analysis with no mass scaling possibility because of the mechanical inertia effects in the forming process. 2D plane strain finite elements with a linear approach for the shape function and with reduced integration are used to model the welding process. A surface-to-surface contact with a penalty penetration method and a finite sliding formulation is chosen for the simulation. The friction formulation is also a penalty method with a coulomb friction coefficient of $\mu=0.15$. Adaptive remeshing is executed with 20 sweeps per increment. The simulated process is velocity-driven at a velocity of 300 m/s. Adiabatic heating effects due to the temperature increase caused by the high inelastic deformations are included in the simulation model. A specific heat per unit mass of $c = 5 * 10^8$ J(tK)$^{-1}$ and a conductivity of $\lambda = 50$ W(mK)$^{-1}$ with an inelastic heat fraction of 0.9 have been assigned to the elements. Due to the high forming velocity the material parameters have to be adjusted to represent the correct material flow behavior. Therefore the plasticity model of Johnson and Cook [6] with a bulk modulus E = 70000 N/mm², a poisson ratio $\upsilon = 0.3$ and a material density $\rho = 2.7 * 10^9$ t mm^{-3} is chosen. In Johnson-Cook constitutive equation, the von-Mises yield stress is given as

$$\sigma = (A + B\varepsilon^n)\,(1 + C\ln\dot{\varepsilon}_p)\,(1 - T^{*m}) \tag{1}$$

where ε is the equivalent plastic strain, $\dot{\varepsilon}_p = \dot{\varepsilon}/\dot{\varepsilon}_0$ is the dimensionless plastic strain-rate for $\dot{\varepsilon}_0 = 1.0/s$, T^* is the homologous temperature $(T - T_{room})/(T_{melt} - T_{room})$, and T is the absolute temperature for $0 \le T^* \le 1.0$ [7]. The five constants are A, B, n, C, and m with the expression in the first set of brackets giving the stress as a function of strain for $\dot{\varepsilon}_p = 1.0$ and $T^* = 0$ and the expressions in the second and third set of brackets representing the effects of strain rate and temperature [7].

The applied Johnson-Cook parameters are listed inTable 3.

Alloy	A	B	n	C	m	E_0
EN AW-6061 T6	275	500	0.3	0.02	1	1

Table 3: Johnson-Cook parameters for Al 6061-T6

The magnification of the contact zone in Figure 9 indicates that the elements close to the contact zone are subject to large strains and high strain rates. Due to the applied Johnson-Cook plasticity model the materials in these locations behave like viscous fluids, resulting in the familiar wavy interface.
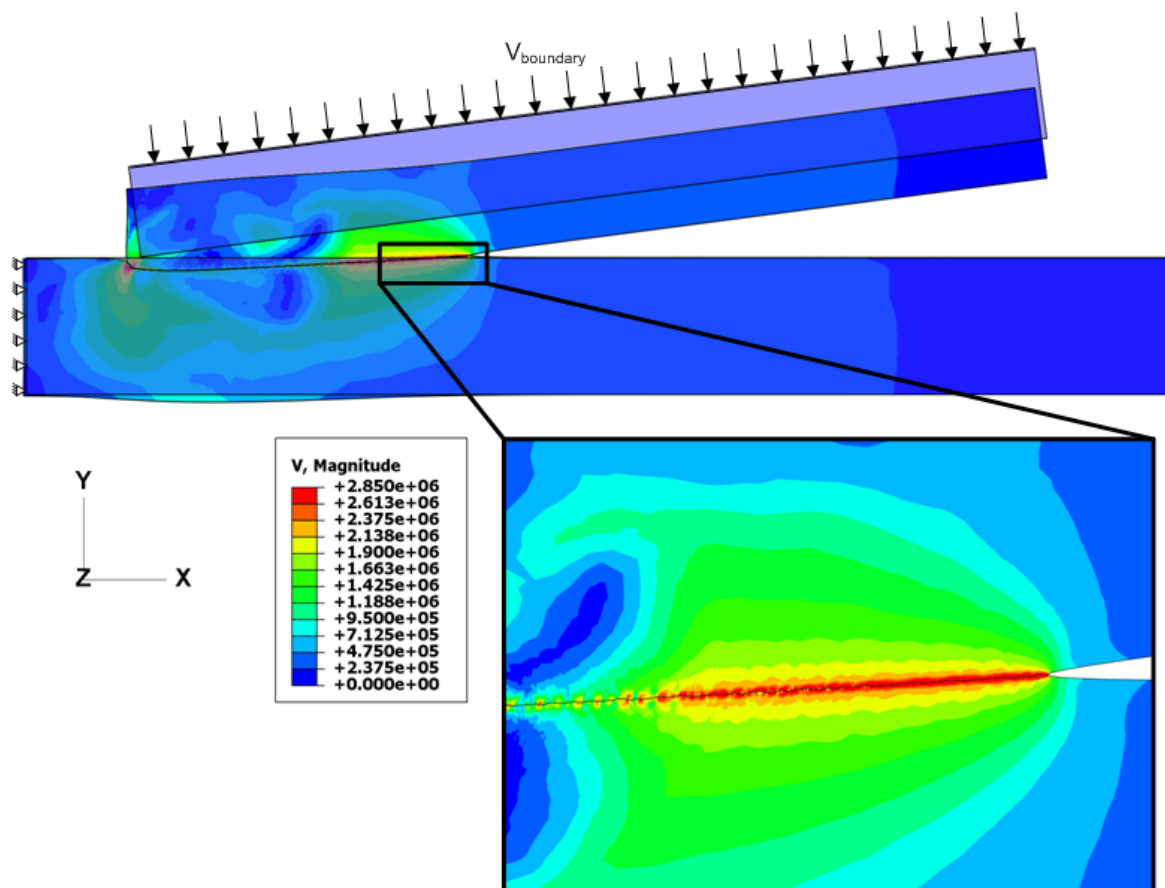

Figure 9: Setup and forming zone of the Finite-Element-model

Results from the numerical simulations of the welding zone are summarized in Figure 10. The welding velocity directly correlates to the impact velocity as indicated by the trigonometrical relation. Regarding wavelength of the interfacial waves, a slight

dependency on the impact velocity can be observed. However, the amplitude of the waves is subject to large variances due to the characteristics of the wave formation mechanism and is highly depending on the mesh properties of the impacting parts.
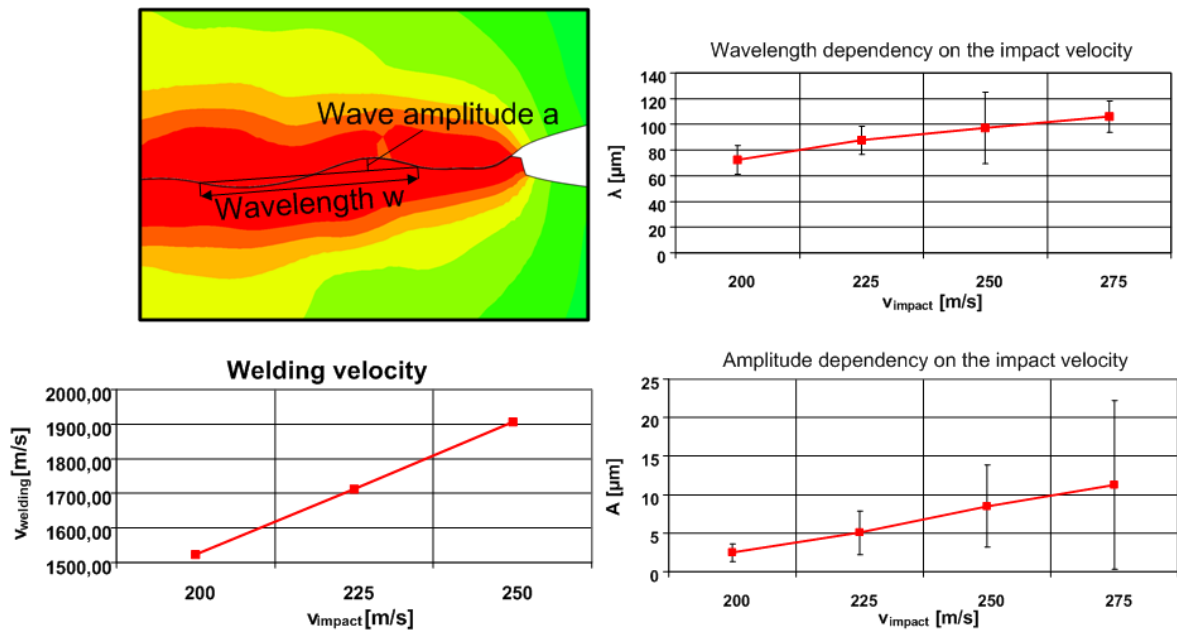

Figure 10: Welding velocity, wavelength and amplitude dependency on the impact velocity

5   Conclusions

In this work experiments have been carried out to identify the process parameters that govern the development of a solid state cold weld in impact welding processes. The impact angle and velocity of the line contact resulting from the trigonometrical relation between the impacting parts and the external pressure have been identified as important parameters for the formation of a welded joint. Metallographic examinations that show a characteristic wavy interface indicated that the material behavior of the surface layers involved is similar to the Kelvin-Helmholtz instability mechanism in fluid dynamics. This material behavior could be mapped in finite element simulations by applying the Johnson-Cook plasticity model.

6   Outlook

The experimental work will proceed in testing further material combinations of aluminum, steel and stainless steel concerning the technological parameters that influence the wave formation and its properties. SEM-imaging and electron microprobe analysis of the interface will be used to give information, whether there appears some kind of mixture or diffusion of the involved materials. These analyses can only be carried out reasonably using dissimilar materials.

The numerical simulations are currently not able to determine whether a bond is likely to occur. Future aspects of the simulative work will focus on contact algorithms that prevent the materials from separating, once threshold values for contact force and strain are exceeded.

References

[1] Aizawa, T.; Kashani, M.; Okagawa, K.: Application of Magnetic Pulse Welding for Aluminium Alloys and SPCC Steel Sheet Joints, Welding Journal, 2007, 86 (5), pp. 119-124

[2] Belyy, I. V.; Fertik, S. M.; Khimenko, L. T.: Electromagnetic Metal Forming Handbook. A Translation of The Russian Book: Spravochnik po Magnitno-impul'snoy Obrabotke Metallov.
Translated By M. M. Altynova, Material Science and Engineering Dept., Ohio State University, 1996

[3] Zhang, P.: Joining Enabled by High Velocity Deformation, Dissertation, Ohio State University, 2003

[4] Robinson, J. L.: The Mechanics of Wave Formation in Impact Welding, Philosophical Magazine, 1975, 31 (3), pp. 587-597

[5] Ben-Artzy, A.; Stern, A.; Frage, N.; Shribman, V.; Sadot, O.: Wave Formation Mechanism in Magnetic Pulse Welding, International Journal of Impact Engineering, 2010, 37, pp. 397-404

[6] Johnson, G. R.; Cook, W. H.: A Constitutive Model and Data for Metals Subjected to Large Strains, High Strain Rates and High Temperatures, Proc. 7th Int. Symp. on Ballistics, The Hague, The Netherlands, 1983

[7] Akbari Mousavi, A. A.; Al-Hassani, S. T. S.: Numerical and Experimental Studies of the Mechanism of the Wavy Interface Formations in Explosive/Impact Welding, Journal of the Mechanics and Physics of Solids, 2005, 53, pp. 2501-252